

Sensitivity Study of Daily Dust Forecast over Mena Region Using RegCM4.4 Model †

Zeinab Salah*

Egyptian Meteorological Authority, Qobry EL-Kobba, Cairo P.O. Box 11784, Egypt

* Correspondence: zeinabsalah@gmail.com

† Presented at the title, place, and date.

Abstract: Dust storms are one of the most frequent weather phenomena in the Middle East and North Africa (MENA) region. Therefore, the daily forecast of dust events is a vital tool for the different sectors. There are many regional models used to forecast atmospheric dust storms. Here, the ICTP regional climate model (RegCM4) was used to simulate atmospheric dust emission, transportation, and deposition, with the optical properties of the dust particles, over the MENA region. In the current work, the Dust Optical Depth (DOD) produced by RegCM4 was compared with the Aerosol Optical Depth (AOD) measured by AERONET over different stations and by MODIS. The first run used two datasets (NCEP/GFS and ERA-Interim) for the meteorological initial and boundary conditions, whereas the second experiment used GFS with two dust emission schemes. The last run used GFS with two values for the erodibility factor (1 and 0.5). The RegCM4 forecast with GFS and Scheme1 resulted in higher values of DOD than that measured by AERONET. However, when using the reanalysis data of ERA-Interim or Scheme2, they did not make a significant difference, but the erodibility factor decreasing has led to reducing the overestimation values.

Keywords: Dust – RegCM4– GFS – ERA-Interim – AOD - erodibility factor

1. Introduction

MENA region is a critical area for developing a better understanding of the factors involved in the generation of large dust events because it is considered a principal source of atmospheric dust, and it exhibits nearly every type of known dust source due to its varied landforms (Middleton and Goudie, 2001; Prospero et al., 2002). However, the data related to the nature of land surfaces in North Africa and the conditions that lead to generating dust storm events are scarce. Numerical models are considered vital tools for forecasting dust storms. Here the Regional Climate Model version 4 hereinafter, “RegCM4.4” (Giorgi et al., 2011), has been run with different meteorological initial and boundary conditions with two dust schemes.

This study aims to improve the daily dust forecast over the MENA region by testing different options in the RegCM4.4 model to determine optimum conditions between them. For this purpose, four experiments have been applied with different criteria, as illustrated later in the following sections.

2. Data and Methodology

2.1. The Dust Model (RegCM4.4)

RegCM4 is a hydrostatic limited area model for a compressible atmosphere, and has been used in various studies of dust emissions in various regions of the world; Asutosh et al. (2021) studied the changes in the dust load over some arid regions in India. Salah et al. (2021) used the RegCM4 model to study the impacts of landuse change on dust

Citation: To be added by editorial staff during production.

Academic Editor: Firstname Last-name

Published: date



Copyright: © 2023 by the authors. Submitted for possible open access publication under the terms and conditions of the Creative Commons Attribution (CC BY) license (<https://creativecommons.org/licenses/by/4.0/>).

emission in Kuwait, and Kuzu and Yavuz (2021) compared the performance of the two dust schemes of RegCM4 over Turkey.

The two dust emission schemes have been used in the current study; the first one (Scheme1) which based on Alfaro and Gomes (2001), Shao (2001), and Zakey et al. (2006), and the other scheme (Scheme2) based on (Kok, 2011a).

In RegCM4.4, the dust mobilization is parameterized as a function of wind speed exceeding a threshold value, surface roughness, minimum friction velocity (Marticorena and Bergametti, 1995), and soil moisture (Fécan et al., 1999), while horizontal mass flux is parameterized in terms of friction velocity by Sun et al. (2012). The dust particles are divided into four size bins (0.1–1.0 μm, 1.0–2.5 μm, 2.5–5.0 μm, and 5.0–20 μm). The radiative flux estimation follows the NCAR-CCM3 scheme (Kiehl et al., 1996). Land surface processes were represented by the biosphere- atmosphere transfer scheme “BATS” (Dickinson et al., 1993). The processes in the planetary boundary layer were parameterized using Holtslag et al. (1990), and the cumulus convection processes were represented by Emanuel (1991). The model includes a large-scale, resolvable subgrid explicit moisture scheme (SUBEX) (Pal et al., 2000).

The studied domain covered North Africa, South Europe, and Middle-East (10° N–60° N, 25° W–60° E) with a resolution of 45km, and 18 vertical sigma levels with the model top set at 50 hPa. The studied period was from 5 May 2014 to 31 May 2014, and each day is a forecast for the next 4 days, but the analysis was done using the first 24 hours from each run.

2.2. Meteorological Data

In this experiment, we used two different sources for the initial and lateral boundary conditions of the atmospheric variables (geopotential height, temperature, relative humidity, and the wind): the first one is the NCEP Global Forecast System (GFS) with a resolution of 1 degree, and the other one is the reanalysis data of ERA-Interim with a resolution of 1.5 degrees, and the lateral boundary conditions are updated every 6 hours.

2.3. AERONET Data

Version 2 Level 1.5 of AERONET products (<https://aeronet.gsfc.nasa.gov/>) were used for the model evaluation over twelve stations, as mentioned in Table 1. The observations were assigned to the nearest hour, and in case more than one observation is assigned to the same hour, the average of all these values was considered. The aerosol optical depth at 550 nm (AOD550) was calculated using AOD at 440, 675, and 870 nm, hereafter (AOD440, AOD675, AOD870) and the Ångström exponent 440-870 (AE440_870) using the Ångström law, as in equation (1).

$$AOD_{550} = \frac{1}{3} \left[AOD_{440} \left(\frac{440}{550} \right)^{AE_{440.870}} + AOD_{675} \left(\frac{675}{550} \right)^{AE_{440.870}} + AOD_{870} \left(\frac{870}{550} \right)^{AE_{440.870}} \right] \quad (\text{eq. 1})$$

Table 1. AERONET stations used in validation.

Number	Station	Lat	Lon
1	Cairo_EMA_2	30.00	31.00
2	Dakar	14.394	-16.959
3	El_Farafra	27.058	27.990
4	Hada_El-Sham	21.802	39.729
5	IER_Cinzana	13.278	-05.934
6	Ilorin	08.00	04.00
7	Izana	28.309	-16.499
8	Ouarzazate	30.928	-06.913

9	Saada	31.626	-08.156
10	SEDE_BOKER	30.855	34.782
11	Tamanrasset_INM	22.00	05.00
12	Zinder_Airport	13.777	08.990

80

2.4. MODIS data

81

The daily means of combined Dark Target and Deep Blue aerosol optical depth at 550 nm for land and ocean calculated from MODIS-Terra and Aqua with resolution 1° x1°, downloaded from (<https://giovanni.gsfc.nasa.gov/giovanni/>), have been used to compare AOD with that forecasted by RegCM4.4. The AOD from MODIS-Terra and MODIS-Aqua were compared with the simulated AOD at the time step of 9 and 12 UTC, respectively, since these two hours are the nearest hours to the time of MODIS.

82

83

84

85

86

87

3. Results and Discussion

88

3.1. Two Different Datasets of the Meteorological Field:

89

Figures (1) show the comparisons of DOD resulting from RegCM4.4 using GFS (red line) and ERA-Interim (green line), and AOD at 550 nm calculated from AERONET measurements using eq. (1) (blue points), in addition to the Ångström Exponent at 440-870 nm (purple points) indicating the particle size (fine or coarse) at the 12 stations listed in Table 1 with the same order.

90

91

92

93

94

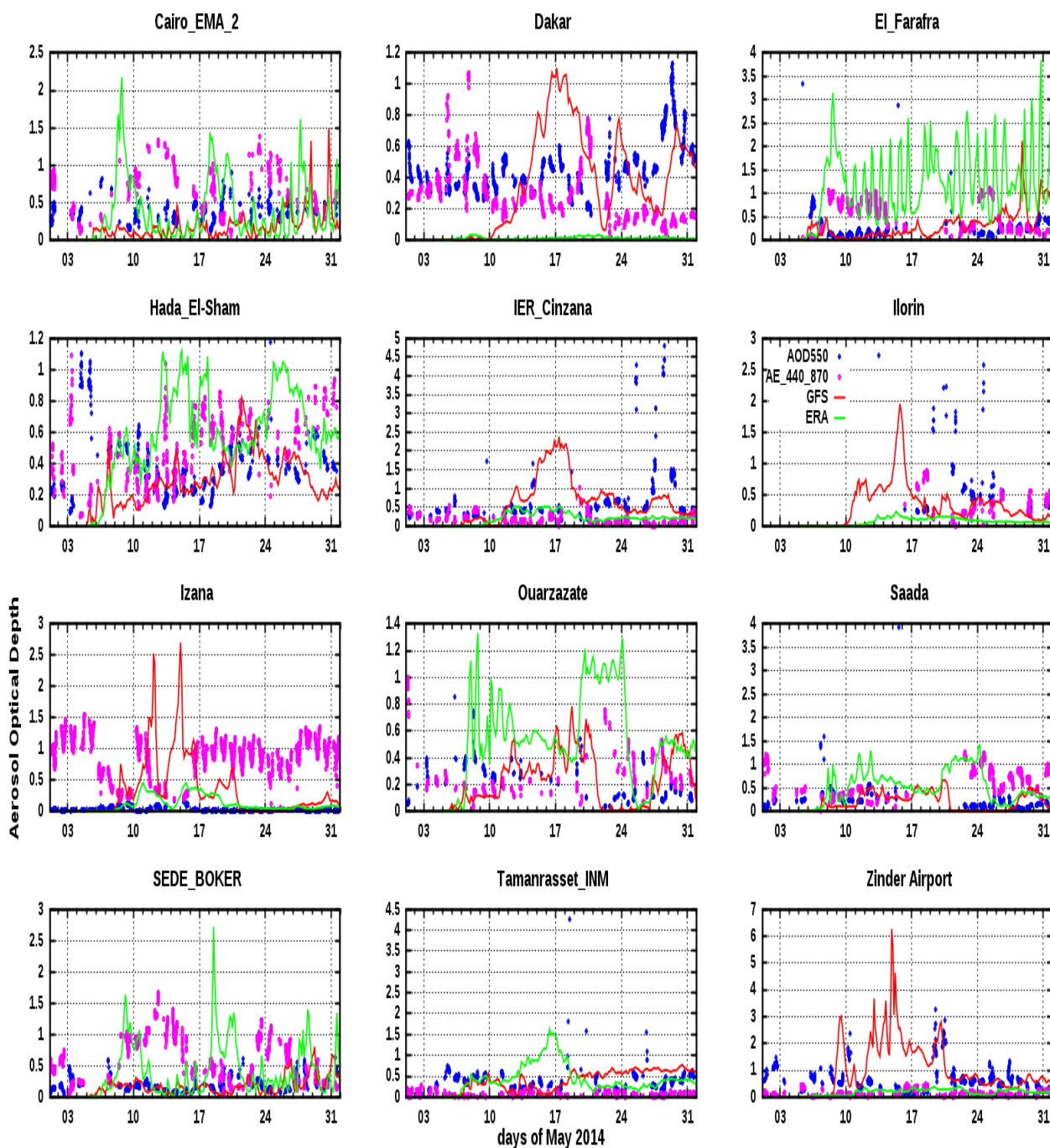


Figure 1. The daily variations of AOD at visible band during May 2014, simulated by RegCM4 with different initial Meteorological fields (red line refers to GFS, and green line refers to ERA-Interim), compared with AOD at 550 nm calculated from AERONET (in blue points) and AE at 440-870 nm (in pink points), over some stations. The figures have been arranged by the same order in table1.

As shown in Figure (1), the behaviors of DOD using GFS and ERA-Interim are not consistent in most cases in the selected stations, however, they provided approximately the same behavior at the station of IER_Cinzana during the period of 14-20 May 2014 with different values of DOD; with GFS DOD exceeded 2, but with ERA-Interim the values were less than 0.5, that is more consistent with the AOD from AERONET. At the station of Izana, DOD resulting from ERA-Interim was near the measured AOD values. Whereas, at the stations of Cairo_EMA_2, Dakar, El_Farafra, Hada_El-Sham, Saada, and SEDE_BOKER, the RegCM4.4 with GFS resulted in DOD values near the observations. Moreover, at Zinder_Airport station, the RegCM4.4 using GFS captured the high values

95

96

97

98

99

100

101

102

103

104

105

106

107

108

of DOD on 9 and 21 May 2014, which agrees with the AERONET, and according to the measured Ångström Exponent (AE) ($AE_{440-870} < 0.5$), which means the high values of AOD is corresponding to dust events, while RegCM4.4 with ERA resulted in lower values of DOD.

3.2. Two Different Dust Emission Schemes:

In this experiment, the RegCM4.4 was run using GFS data with the two dust emission schemes. Figures (2) show the DOD produced by RegCM4.4 with the scheme1 (in red line), DOD of the scheme2 (in green line), AERONET AOD at 550 nm (blue points), and the Ångström Exponent at 440-870 nm (purple points). One can notice that the two schemes produced the same behavior over all stations but with different values of dust optical depth, as in the stations of Cairo_EMA_2 and El_Farafra on the days of 29 and 31 May 2014, when the DOD with scheme1 exceeded 1, whereas scheme2 was more consistent with AOD from AERONET. In the station of IER_Cinzana, the two schemes resulted in more dust causing high values of DOD to exceed 1.5 in the period of 15-19 May 2014, whereas the AERONET AOD values were ≤ 0.5 . Moreover, the same feature repeated with the station of Izana during 10-22 May 2014 and the station of Zinder_Airport during 12-19 May 2014.

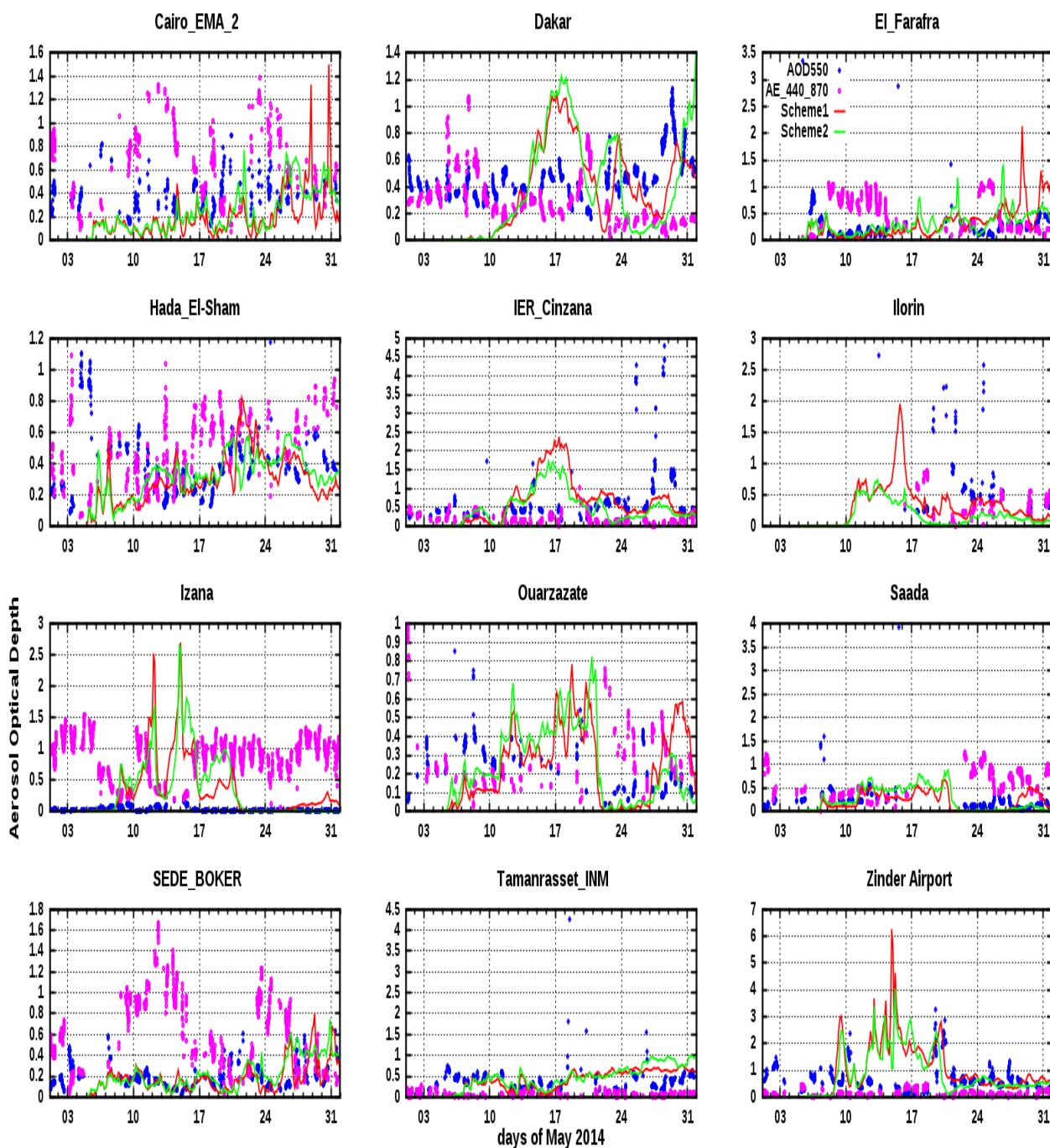


Figure 2. The daily variations of AOD at visible band during May 2014, simulated by RegCM4 with different emission schemes (red line refers to Scheme1, and green line refers to Scheme2), compared with AOD at 550 nm calculated from AERONET (in blue points) and AE at 440-870 nm (in pink points), over some stations. The figures have been arranged by the same order in table1.

3.3. Two Values for Dust Emission Adjustment Factor:

The dust flux is directly proportional to the fraction of the erodible surface (E), which is related to the fraction of the uncovered surface by the roughness elements and exposed to wind erosion. Laurent et al. (2006) showed that the fraction of erodible surface roughly decreases as a function of the roughness length (Z0) in the desert regions. For Z0 less than 3×10^{-3} cm, the desert surface can be considered as totally erodible ($E = 1$), whereas when Z0 exceeds 3×10^{-3} cm, E can be calculated as a linear function of the logarithm of Z0 as the equation of Laurent et al. (2008):

126
127
128
129
130
131
132
133
134
135
136
137
138
139

$$E = 0.7304 - (0.0804 \times \log_{10}(ZO)) \tag{2}$$

In this experiment, the RegCM4.4 model was run using GFS data and scheme1, but with two values of dust emission adjustment factor (or soil erodibility); 1 and 0.5. Figures (3) show the DOD produced by RegCM4.4 assuming the adjustment factor equals 1 and 0.5, represented in red line and green, respectively, AERONET AOD at 550 nm (in blue points), and the Ångström Exponent at 440-870 nm (purple points).

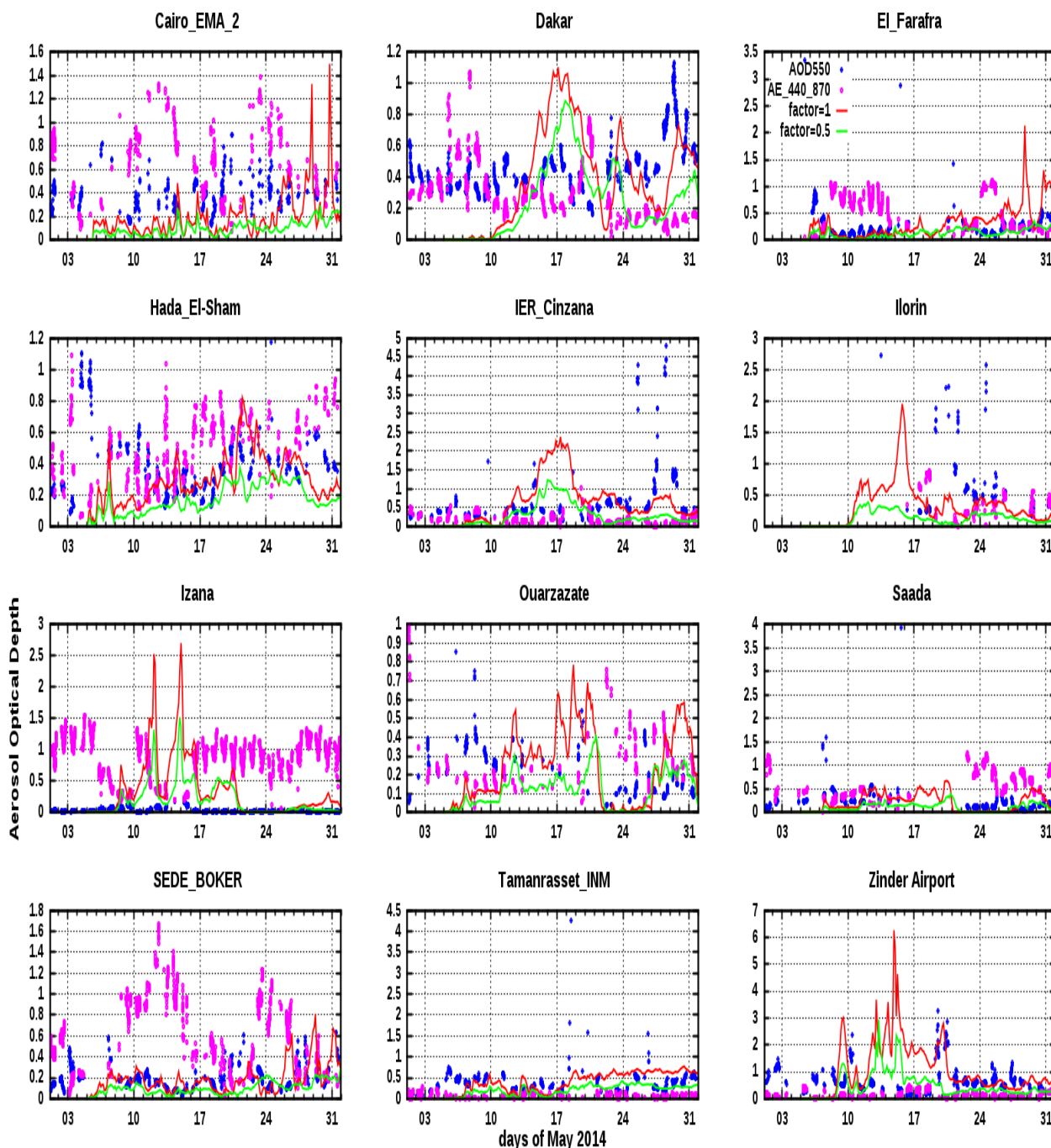


Figure 3. The daily variations of AOD at visible band during May 2014, simulated by RegCM4 with different values of erodibility factor (red line refers to value of 1, and green line refers to value of 0.5), compared with AOD at 550 nm calculated from AERONET (in blue points) and AE at 440-870 nm (in pink points), over some stations. The figures have been arranged by the same order in table1.

140
141
142
143
144

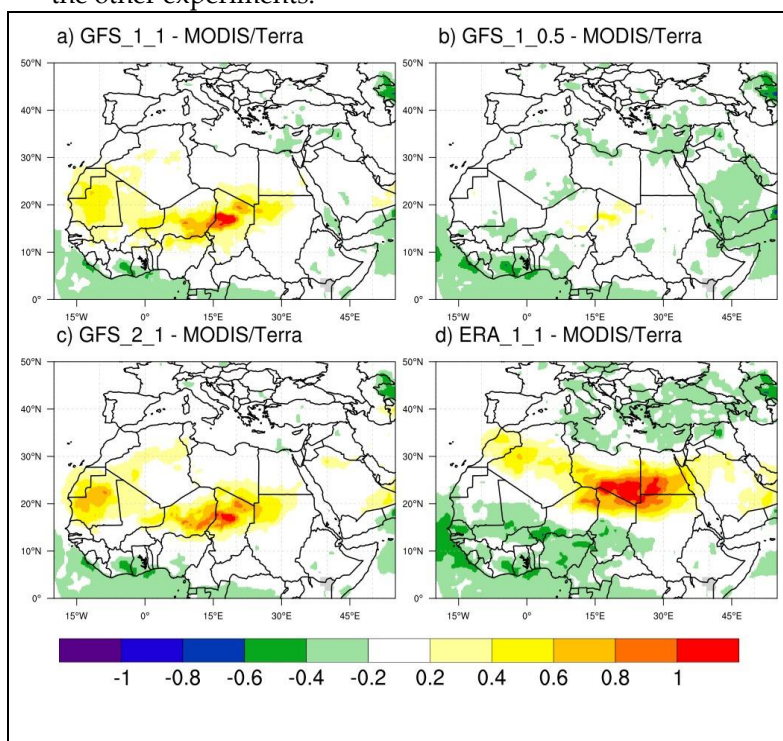
145
146
147
148
149
150

From the previous experiments, one can notice the problem of the high values of AOD that exceeded two in some cases in contrast with that extracted by AERONET. Therefore, these values can give the false alarm of a severe dust storm.

The changes in the erodibility factor had an effective influence on the DOD values. Using the erodibility factor of 0.5 resulted in a noticeable decrease of the DOD at the stations of Cairo_EMA_2 and El-Farafra, in the last days of May, in addition to the stations of IER_Cinzana, Izana, Ouarzazate, and Zinder_Airport, in the middle of May.

3.4. Comparison against MODIS/Aqua Measurements

The average of the whole studied period was calculated for the AOD of MODIS-Terra and Aqua, and then the bias was calculated between the DOD produced from RegCM4.4 at 9 and 12 UTC with measured AOD from Terra and Aqua, respectively, as shown in Figure (4). It can be noticed that AOD resulting from the GFS_1_0.5 experiment (GFS data and the scheme1 with erodibility factor=0.5) caused less bias over Sahara compared with the other experiments.



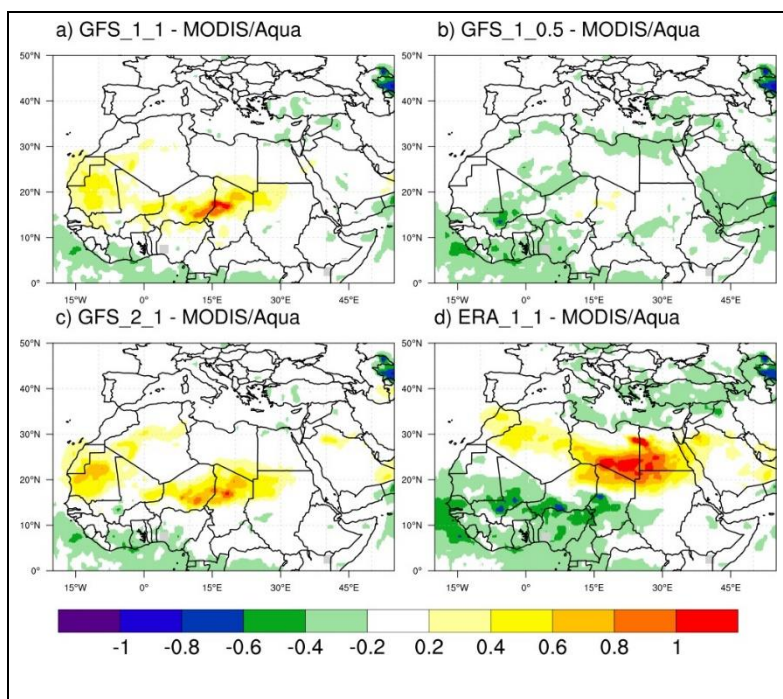


Figure 4. The bias of average AOD over the whole studied period, simulated by the four different experiments: a) GFS_1_1 (GFS and scheme1 with erodibility factor =1); b) GFS_1_0.5 (GFS and scheme1 with erodibility factor =0.5); c) GFS_2_1 (GFS and scheme2 with erodibility factor =1), d) ERA_1_1 (ERA-Interim and scheme1 with erodibility factor =0.5), with respect to the AOD from MODIS/Terra in above two rows, and MODIS/Aqua in the down rows.

4. Conclusions

In this study, different options have been used to run the model of RegCM4.4 to forecast dust emissions over the MENA region. These options included: 1) two meteorological fields: the NCEP-GFS forecast and ERA-Interim reanalysis, 2) two different dust emission schemes, and 3) two values of the soil erodibility factor. These experiments were limited to only one month of daily dust forecast.

The higher values of dust optical depth were the most noticeable problem in our forecast. Therefore, through some tests of different options, the change of the erodibility factor values with the first dust scheme caused a significant reduction of AOD on some AERONET stations. Also, the two dust emission schemes produced the same behavior over all stations but with different values of dust optical depth.

Finally, it needs more experiments with different planetary boundary layer schemes, land surface models, convection schemes, and radiation schemes available in RegCM4.4 for a long period to improve the forecast of dust emissions using RegCM4.4.

Acknowledgments: The author thanks the PI investigators and their staff for establishing and maintaining the AERONET sites used in this investigation.

Conflicts of Interest: The authors declare no conflict of interest.

References

- Alfaro, S. C. and Gomes, L.: Modeling mineral aerosol production by wind erosion: Emission intensities and aerosol size distribution in source areas, *J. Geophys. Res.*, 106, 18075–18084, doi:10.1029/2000JD900339, 2001.
- Asutosh, Acharya, S.K Pandey, V Vinoj, Ramakrishna Ramisetty, and Nishant Mittal. 2021. "Assessment of Recent Changes in Dust over South Asia Using RegCM4 Regional Climate Model" *Remote Sensing* 13, no. 21: 4309. <https://doi.org/10.3390/rs13214309>
- Dickinson RE, Henderson-Sellers A, Kennedy PJ 1993. Biosphere– atmosphere transfer scheme (BATS) version 1E as coupled to the NCAR Community Model. In: NCAR Technical report. TN-387+STR, NCAR, Boulder, CO

4. Emanuel K (1991) A scheme for representing cumulus convection in large scale models. *J Atmos Sci* 48: 2313–2335. 196
5. Fécan, F., B. Marticorena, and G. Bergametti. (1999). Parameterization of the increase of the aeolian erosion threshold wind friction velocity due to soil moisture for arid and semi-arid areas. *Annales Geophysicae*, 17, 149–157. 197
6. Giorgi F, et al. (2011). RegCM4: Model description and illustrative basic performance over selected CORDEX domains. Submitted to *Climate Research*. 199
7. Holtzlag A, de Bruijn E, Pan HL (1990). A high resolution air mass transformation model for short range weather forecasting. *Mon Weather Rev* 118: 1561–1575. 200
8. Kiehl J, Hack J, Bonan G, Boville B, Briegleb B, Williamson D, Rasch P 1996. Description of the NCAR community climate model (CCM3). In: NCAR Technical report. TN-420+STR, NCAR, Boulder, CO. 201
9. Kok, J. F.(2011a). A scaling theory for the size distribution of emitted dust aerosols suggests climate models underestimate the size of the global dust cycle, *P. Natl. Acad. Sci. USA*, 108, 1016–1021, doi:10.1073/pnas.1014798108. 202
10. Kuzu, S.L., Yavuz, E. Comparison of RegCM dust schemes by monitoring an aeolian dust transport episode. *Air Qual Atmos Health* 14, 2047–2057 (2021). <https://doi.org/10.1007/s11869-021-01073-z> 203
11. Laurent, B., B. Marticorena, G. Bergametti, and F. Mei (2006), Modeling mineral dust emissions from Chinese and Mongolian deserts, *Global Planet. Change*, 52(1– 4), 121– 141. 204
12. Laurent, B., B. Marticorena, G. Bergametti, J. F. Le ‘on, and N. M. Mahowald (2008), Modeling mineral dust emissions from the Sahara desert using new surface properties and soil database, *J. Geophys. Res.*, 113, D14218, doi: 10.1029/2007JD009484. 205
13. Marticorena, B., and G. Bergametti (1995), Modeling the atmospheric dust cycle: 1. Design of a soil derived dust production scheme, *J. Geophys. Res.*, 100, 16,415– 16,430. 206
14. Middleton, N.J., and A.S. Goudie (2001), Saharan dust: sources and trajectories, *Trans. Inst. Br. Geogr.*, 26, 165–181. 207
15. Pal, J. S., E. E. Small, and E. A. B. Eltahir, Simulation of regional-scale water and energy budgets: Representation of subgrid cloud and precipitation processes within RegCM, *J. Geophys. Res.-Atmospheres*, 105(D24), 29,579–29,594, 2000. 208
16. Prospero, J.M., P. Ginoux, O. Torres, S.E. Nicholson, and T.E. Gill (2002), Environmental characterization of global sources of atmospheric soil dust identified with the Nimbus 7 Total Ozone Mapping Spectrometer (TOMS) absorbing aerosol product, *Rev. Geophys.*, 40, 1002, doi:10.1029/2000RG000095. 209
17. Salah, Z., Dashti, H., Zakey, A. et al. How land use change can improve air quality status over Kuwait. *Int. J. Environ. Sci. Technol.* 19, 747–762 (2022). <https://doi.org/10.1007/s13762-021-03171-y> 210
18. Shao, Y. (2001), A model for mineral dust emission, *J. Geophys. Res.*, 106(D17), 20,239–20,254, doi:10.1029/2001JD900171. 211
19. Sun, H., Pan, Z., Liu, X., 2012. Numerical simulation of spatial–temporal distribution of dust aerosol and its direct radiative effects on East Asian climate. *J. Geophys. Res.* 117 (D13), 1–14. <http://dx.doi.org/10.1029/2011JD017219>. 212
20. Zakey, A. S., Solmon, F., and Giorgi, F.: Implementation and testing of a desert dust module in a regional climate model, *Atmos. Chem. Phys.*, 6, 4687–4704, doi:10.5194/acp-6-4687-2006, 2006. 213

Disclaimer/Publisher’s Note: The statements, opinions and data contained in all publications are solely those of the individual author(s) and contributor(s) and not of MDPI and/or the editor(s). MDPI and/or the editor(s) disclaim responsibility for any injury to people or property resulting from any ideas, methods, instructions or products referred to in the content. 214